Are nitrous oxide emissions indirectly fueled by input of terrestrial dissolved organic nitrogen in a large eutrophic Lake Taihu, China?

Yongqiang Zhou [a,b,1], Qitao Xiao [a,b,1], Lei Zhou [a,b], Kyoung-Soon Jang [c], Yunlin Zhang [a,b,*], Mi Zhang [d], Xuhui Lee [d], Boqiang Qin [a,b], Justin D. Brookes [e], Thomas A. Davidson [f], Erik Jeppesen [f,g]

[a] State Key Laboratory of Lake Science and Environment, Nanjing Institute of Geography and Limnology, Chinese Academy of Sciences, Nanjing 210008, China
[b] University of Chinese Academy of Sciences, Beijing 100049, China
[c] Biomedical Omics Center, Korea Basic Science Institute, Cheongju 28119, South Korea
[d] Yale-NUIST Center on Atmospheric Environment, International Joint Laboratory on Climate and Environment Change (ILCEC), Nanjing University of Information Science and Technology, Nanjing 210044, China
[e] Water Research Centre, Environment Institute, School of Biological Science, University of Adelaide, 5005 Adelaide, Australia
[f] Department of Bioscience and Arctic Research Centre, Aarhus University, Vejlsøvej 25, DK-8600 Silkeborg, Denmark
[g] Sino-Danish Centre for Education and Research, Beijing 100190, China

HIGHLIGHTS

- Terrestrial DON input in the inflowing river mouths likely enhanced ammonification.
- DOM degradation in the inflow-affected areas fuels oxygen consumption.
- DO depletion fuels incomplete aerobic nitrification and nitrifier-denitrification.
- Terrestrial DON input potentially fueling N_2O efflux from Lake Taihu.

GRAPHICAL ABSTRACT
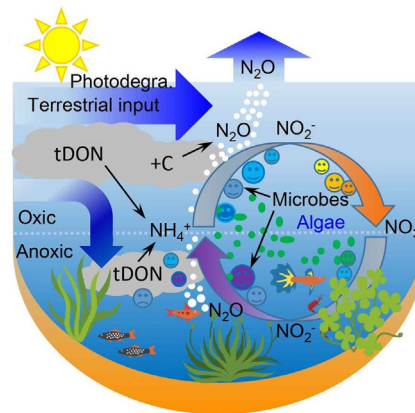
ARTICLE INFO

ABSTRACT

Lakes actively transform nitrogen (N) and emit disproportionately large amounts of N_2O relative to their surface area. Studies have investigated the relative importance of denitrification or nitrification on N_2O emissions; however, the linkage between N_2O efflux and dissolved organic nitrogen (DON) and carbon (DOC) remains largely unknown. Long-term (2012–2017) seasonal field observations and a series of degradation experiments were used to unravel how DON composition impacts N_2O emissions from Lake Taihu, China. In the northwestern part of the lake, large riverine inflow and high N_2O emissions occur in all seasons (24.6 ± 25.2 μmol m^{-2} d^{-1}), coincident with high levels of terrestrial DON and DOC here. The degradation of labile DON and DOC likely enhanced ammonification as supported by the correlations between NH_4^+-N and DON, DOC, a(350), and terrestrial humic-like C3. The area with large riverine inputs in the northwestern part of the lake was characterized by low

DO which may enhance incomplete aerobic nitrification and incomplete denitrification, both leading to N_2O production. Twenty days laboratory experiments indicated greater N_2O production in the northwest inflow samples (N_2O on day 20: 120.9 nmol L^{-1} and 17.3 nmol L^{-1} for bio- and photo-degradation samples, respectively) compared with the central lake samples (N_2O on day 20: 20.3 nmol L^{-1} and 12.3 nmol L^{-1} for bio- and photo-degradation samples, respectively), despite both having low Chl-*a*. Our DON and DOC degradation experiments confirmed the occurrence of ammonification along with consumption of NH_4^+-N and thereafter NO_3^--N. Our results collectively suggest that terrestrial DON fueled ammonification, enhanced nitrification and incomplete denitrification, and thereby became an important contributor to the N_2O efflux from Lake Taihu.

1. Introduction

Lakes cover <4% of the non-glaciated global surface; yet, they actively transform carbon and nitrogen and outgas a disproportionately large amount of greenhouse gases relative to their surface area (Soued et al., 2015; Davidson et al., 2018). Carbon dioxide (CO_2) and methane (CH_4) emissions from lakes have been extensively studied to evaluate the global and regional C budget (Davidson et al., 2015; Weyhenmeyer et al., 2015; Wik et al., 2016; Aben et al., 2017; Wen et al., 2017). Nitrous oxide (N_2O) has a global warming potential of 300 times that of CO_2 on a century scale and is a major component responsible for stratospheric ozone depletion (Griffis et al., 2017). The N_2O concentration in the atmosphere has increased rapidly from 270 parts per billion (ppb) before the industrial revolution to 319 ppb in 2005 with a linear increasing rate of ~ 0.8 ppb yr^{-1} during the past few decades (Davidson, 2009). Anthropogenic activities, especially agricultural utilization of synthetic fertilizers, have impacted the nitrogen balance in lake ecosystems, potentially leading to enhanced emission of N_2O (Davidson, 2009). However, our understanding of the efflux of N_2O from freshwater ecosystems and the associated driving factors are fragmentary (Soued et al., 2015). The large riverine nitrogen input to lakes from residential and agricultural catchments represents a potential, but often ignored, source of N_2O (Soued et al., 2015; Xiao et al., 2018). Studies have indicated that N_2O is a byproduct of nitrification (NH_4^+-N → NO_2^--N → NO_3^--N) or an intermediate byproduct of microbial denitrification (NO_3^--N → NO_2^--N → NO→N_2O → N_2) (Jetten, 2008; Elberling et al., 2010; Beaulieu et al., 2011; Soued et al., 2015; Kuypers et al., 2018; Xiao et al., 2018). For example, a recent study revealed that N_2O efflux correlated positively with NH_4^+-N ($r^2 = 0.20$, $p < 0.001$), NO_3^--N ($r^2 = 0.09$, $p < 0.01$) in Lake Taihu during 2012–2015 (Xiao et al., 2018) (Fig. S1), although much of the variation in the N_2O efflux remains unexplained. Current estimates of the N_2O efflux assume that there is a linear relationship between N_2O and dissolved inorganic nitrogen (DIN, i.e. the sum of NH_4^+-N, NO_3^--N, and NO_2^--N), but the relationship, where present, is weak across ecosystem types (Soued et al., 2015). The uncertainty of estimates of the lacustrine N_2O efflux is due, in part, to a paucity of monitoring data and lack of knowledge about the underlying processes.

Rivers draining urban residential areas may carry significant inputs of dissolved organic nitrogen (DON), carbon (DOC), and N_2O via household sewage effluents. The occurrence of N_2O emission hotspots in lakes could be induced by hyporheic zone nitrification and denitrification (Hu et al., 2016), effluents from upstream wastewater treatment plants (Beaulieu et al., 2011; Yu et al., 2013), and DON degradation caused by in situ N_2O production. N loading and forms (e.g. NH_4^+-N or NO_3^--N), dissolved oxygen (DO), pH, bio-labile DOC, water temperature, and water depth have been suggested to strongly influence the N_2O efflux (Beaulieu et al., 2011; Yu et al., 2013; Hu et al., 2016). Specifically, elevated NH_4^+-N concentrations coupled with hypoxia may determine the N_2O efflux in urbanized watersheds (Rosamond et al., 2012; Yu et al., 2013), and also stream order and land use correlated with the N_2O efflux (Beaulieu et al., 2011; Turner et al., 2015). Ammonification resulting from microbial and photochemical degradation of DON, an important and highly bio-labile fraction of nitrogen in lake water (Lusk

and Toor, 2016a; Lusk and Toor, 2016b; Huang et al., 2018), may lead to significant release of NH_4^+-N. NH_4^+-N oxidation undertaken by autotrophic ammonia oxidasing bacteria thereafter enhances N_2O production via aerobic nitrification or nitrifier denitrification (NH_4^+-N oxidation to NO_2^--N followed by reduction to N_2O and N_2) (Cébron et al., 2005). Nitrification and denitrification reaction kinetics are determined directly by the terminal electron donors (NH_4^+-N, bio-labile DON and DOC) and acceptors (DO and NO_3^--N) (Zarnetske et al., 2012). In shallow eutrophic lakes, the input of high concentrations of DON and DOC, coupled with the relatively long water residence time and enhanced microbial reworking of DON and DOC, implies that bio-labile DON (DOC) and DO could serve as electron donors and acceptors, respectively (Jetten, 2008; Hu et al., 2016; Kuypers et al., 2018). DO consumption resulting from the degradation of organic substances (bio-labile DOC and DON) likely lead to incomplete aerobic nitrification, which can eventually result in excessive production of N_2O (Jetten, 2008; Elberling et al., 2010; Soued et al., 2015; Xiao et al., 2018). However, to date, no attempt has been made to investigate the linkages between the lacustrine N_2O efflux with the sources and composition of DON.

DON is an important fraction of total dissolved nitrogen (TDN) in lake ecosystems and is composed of a variety of organic compounds including amino acids associated with protein-like substances, urea, and humic-rich materials (Lusk and Toor, 2016a; Lusk and Toor, 2016b; Osburn et al., 2016). In eutrophic waters, the microbial community is rapidly cycling a labile DOM sub-fraction (Zhang et al., 2009), and this is difficult to detect using chemical measurements due to its rapid uptake (Stedmon et al., 2007). Nitrogen binds to aromatic substances and amino acids directly impacting humic-like and protein-like fluorescence properties, respectively, making DOM fluorescence relevant for DON measurements (Heinz et al., 2015; Osburn et al., 2016). New advanced analytical techniques including ultrahigh resolution mass spectrometry (FT-ICR MS and FT-Orbitrap MS) provide the necessary tools for examining the relative importance of DON molecular composition in fueling N_2O emission.

The objective of this study was to unravel how the sources and composition of DON may impact the emission of N_2O from aquatic ecosystems. The work was undertaken at Lake Taihu in China, which is a good candidate for this kind of analysis as it is a large shallow eutrophic lake with high heterogeneity of both DON and N_2O efflux (Xiao et al., 2018; Zhou et al., 2018b). Long-term seasonal (February 2012–November 2017) measurements of DON, DIN, DOM absorption, fluorescence, stable isotopic $\delta^{15}N$-TDN, and $\delta^{18}O$ coupled with FT-ICR MS derived from the samples collected from the lake as well as a series of laboratory DON degradation experiments were employed to investigate how the sources of DON may impact the emission of N_2O. As the lake's watershed is intensely urbanized and cultivated, we hypothesized that the labile terrestrial DON input likely enhances ammonification and that bio-labile DOC and DON act as terminal electron donors, their degradation probably resulting in oxygen depletion in the inflowing river mouths. We therefore hypothesized that degradation of DON from the lake watershed leads to enhanced incomplete aerobic nitrification and nitrifier denitrification, and thereby emission of N_2O from the lake.

2. Materials and methods

2.1. Study sites and field sampling

Lake Taihu is a large, shallow, and highly eutrophic lake located in the lower reach of the Yangtze River Basin. The lake has an area of 2338.1 km^2 and a mean depth of 1.89 m. A total of 172 rivers or channels are connected to the lake, and the lake's watershed can be divided into seven sub-watersheds: Huxi, Wuchengxiyu, Zhexi, Hangjiahu, Yangchengdianmao, Puxi, and Pudong (Fig. 1) according to the hydraulic connections of the watershed river networks (Qin et al., 2007; Zhou et al., 2018c). The sub-watersheds of Puxi and Pudong do not surround the lake (Fig. 1). Data on monthly net inflow discharge from the five sub-watersheds surrounding the lake from 2012 to 2016 can be found in Zhou et al. (2018c). Information on land use in the lake watershed was extracted from 1 km resolution national land cover data for China based on Landsat images (available from http://www.resdc.cn/) using ArcGIS 10.2 software. Inflowing rivers from the northwestern Huxi and northern Yangchengdianmao sub-watersheds are dominated by urban and agricultural land use and they discharge substantial terrestrial nutrients and anthropogenic effluents, enriched in DON, to the lake. As a result, the northwestern Zhushan and northern Meiliang Bay experience severe eutrophication (Qin et al., 2007; Zhou et al., 2018b). In comparison, submerged macrophytes dominate in the southeastern outflowing bays (Qin et al., 2007).

A total of 829 surface water samples (~0.5 m) were collected from Lake Taihu, including 768 samples taken at 32 lake sites over the season (February, May, August, and November) from February 2012 to November 2017 (6 years × 4 seasons × 32 sites) and a campaign in Zhushan Bay (n = 61 sites) in May 2014. DO concentrations and water temperature were determined in situ using a YSI 6600 multi-parameter water quality sonde (Yellow Springs Inc., OH, USA). Water samples (0.5 m, ~5 L) were collected using water samplers lowered into the lake, stored on ice, and kept in darkness while in the field. Samples were transported to the laboratory where they were filtered immediately upon arrival and then stored in the dark at 4 °C. DOM absorption and fluorescence measurements were typically undertaken within three days, all laboratory measurements were completed in five days, and filtrates were immediately frozen at −20 °C for stable isotopic δ^{15}N-TDN and FT-ICR MS.

Light attenuation measurements were performed during the campaign in the north-western inflowing Zhushan Bay in May 2014 to investigate if photochemical degradation may enhance the transformation of DON in the lake region. Detailed information on the measurements of the diffuse attenuation coefficient of downwelling irradiance, $K_d(\lambda)$, especially ultraviolet radiation, in the inflowing river mouths can be found in the Supporting Information and elsewhere (Zhou et al., 2018b).

2.2. DON concentration, CDOM absorption, and fluorescence measurements

DON concentrations were determined by subtraction of NH_4^+-N, NO_3^--N, and NO_2^--N from TDN, and water samples for determination of TDN concentration were filtered through Whatman GF/F filters (0.7 μm porosity) measured at a wavelength of 210 nm using a Shimadzu UV-2550PC UV–Vis spectrophotometer after digestion (Xiao et al., 2018). NH_4^+-N, NO_3^--N, and NO_2^--N concentrations were determined with a flow injection (Skalar SAN++, Delft, Netherlands) analyzer. DON, NH_4^+-N, NO_3^--N, and NO_2^--N results were available for the lake water samples seasonally from February 2012 to November 2017.

Detailed information on CDOM absorption can be found in the Supporting Information. Absorption at 254 and 350 nm, i.e. $a(254)$ and $a(350)$, have been widely used as proxies of the CDOM concentration in various environments (Stedmon et al., 2007; Spencer et al., 2013; Yang and Hur, 2014; Zhou et al., 2018a) and are therefore used in this study. CDOM spectral slope ($S_{275-295}$) was estimated from the absorption spectra with nonlinear fitting, and $S_{275-295}$ together with the absorption ratio $a(250):a(365)$ increase with decreasing terrestrial soil organic-rich signals (Helms et al., 2008; Fichot and Benner, 2012). The specific ultraviolet absorbance at 254 nm (SUVA$_{254}$) of DOC is a reliable indicator of the aromaticity of CDOM (Spencer et al., 2012; Yang and Hur, 2014; Zhou et al., 2018a).

DOM fluorescent excitation-emission matrices (EEMs) coupled with parallel factor analysis (PARAFAC) have been used to trace the dynamics of the optical composition of DOM (Stedmon and Markager, 2005; Yang et al., 2012; Murphy et al., 2013; Guo et al., 2014; Yang et al., 2017; Song et al., 2018), and also specifically DON (Osburn et al., 2016; Hounshell et al., 2017) in various natural aquatic ecosystems. Detailed information on DOM fluorescence excitation-emission matrices (EEMs) measurements and calibration can be found in the Supporting Information. Daily variations of lamp intensity were normalized to corresponding daily Milli-Q water Raman peaks of EEMs at Ex = 350 nm and yield EEMs intensities in Raman unit (R.U.) (Lawaetz and Stedmon, 2009). Data on CDOM absorption and fluorescence for the samples collected from Zhushan Bay in May 2014 and the seasonal sampling campaign in the lake in 2012–2016 can be found in the literature (Zhou et al., 2018b; Zhou et al., 2018c). The fluorescence peak integration ratio of
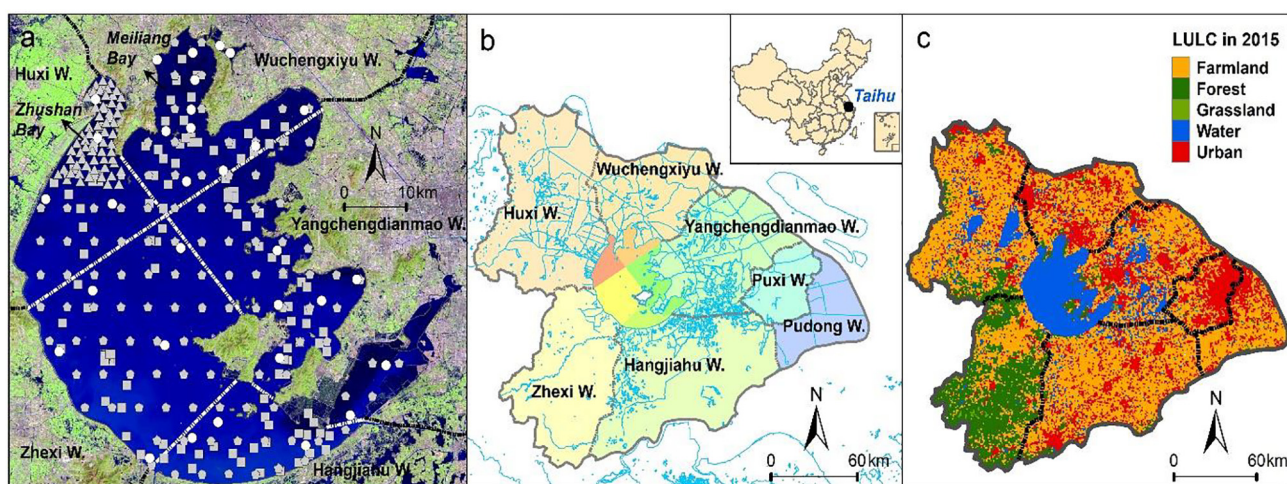

Fig. 1. Location of Lake Taihu seasonal sampling sites (February, May, August, and November, white circles, n = 32) from 2012 to 2017, and 61 sites sampled in Zhushan Bay in May 2014 (gray triangles). The location of supplementary 116 sites sampled in January and June 2014 and in June 2015 (gray pentagons) and 146 sites in October 2008 (gray squares) are also shown (a). All the sampling sites were divided into five spatial groups delineated by white lines following the boundaries of the corresponding sub-watersheds (Huxi, Wuchengxiyu, Zhexi, Hangjiahu, and Yangchengdianmao) (b). Land use and land cover (LULC) in the Lake Taihu watershed in 2015 (c).

Peak C to Peak T, i.e. $I_C:I_T$, can be used to trace the relative importance of terrestrial or autochthonous DOM, and the ratio increased with enhanced aromaticity of DOM (Zhou et al., 2017).

2.3. N₂O sample collection, measurements, and efflux calculation

A total of 760 headspace samples were collected from the lake seasonally from February 2012 to November 2017 (29 sampling sites × 4 seasons × 6 years) and in August and November 2018 (32 sampling sites × 2 seasons) to determine dissolved N_2O concentrations (Fig. 1). Detailed information on the sampling procedures and subsequent measurements can be found in the Supporting Information.

Dissolved N_2O concentrations were analyzed following the headspace equilibration approach detailed in Davidson et al. (2015) and Xiao et al. (2018) and can be found in the Supporting Information. Data on the N_2O efflux in the lake in 2012–2015 can be found in Xiao et al. (2018).

2.4. Measurements of bacterial abundance, chlorophyll-a (Chl-a), DOC, and chemical oxygen demand (COD)

Total bacterial abundance was determined for water samples collected seasonally from the lake between February 2012 and November 2014 (3 years × 4 seasons × 32 sites) using an epifluorescence microscopy approach detailed in Tang et al. (2010). Seasonal COD concentrations were determined from February 2012 to November 2017 following a colorimetric method with potassium dichromate and sulfuric acid as reagent. Chl-a concentrations were measured spectrophotometrically at 665 and 750 nm after extraction with hot ethanol (90% at 80 °C) (Song et al., 2018) and were available for the lake water samples seasonally from February 2012 to November 2017; data on Chl-a in 2012–2016 can be found in the literature (Zhou et al., 2018c). DOC concentrations in filtrates passed through GF/F filters were determined on a TOC-V CPN (Shimadzu, Tokyo, Japan) analyzer at high temperature (680 °C) after acidification with 10 μL of 85% H_3PO_4 (Zhou et al., 2018c). Data on DOC were unavailable for the water samples collected before February 2013 except for the sampling campaign conducted in October 2008, and data on DOC in 2013–2016 can be found elsewhere (Zhou et al., 2018c).

2.5. Stable isotopic $\delta^{18}O$ and $\delta^{15}N$-TDN measurements

Evaporation enhances the accumulation of the heavy isotopic water molecule $H_2\delta^{18}O$ in surface lake water (Wu et al., 2015), and $\delta^{18}O$ can therefore be used to trace the sources and variability of water and terrestrial CDOM. Surface water samples (~0.1 m) were seasonally collected from the 32 sites in the lake (February, May, August, and November) from February 2012 to November 2014 (3 years × 4 seasons × 32 sites). Details about the sampling and pre-processing for analysis of the stable isotope $\delta^{18}O$ can be found elsewhere in Xiao et al. (2016) and Zhou et al. (2018b), and in the Supporting Information. $\delta^{15}N$-TDN coupled with $\delta^{13}C$-DOC was determined for the samples collected from the lake in November 2016 (n = 32) to trace the source of N in the lake and the data can be found elsewhere (Zhou et al., 2018c) and in the Supporting Information.

2.6. Bio- and photo-degradation experiments

DOM bio-lability is the degree to which DOM is available for microbial mineralization, and biodegradable DOM (BDOM) is defined as the percent of DOM uptake over a certain time period, mostly 14–28 days (Hood et al., 2009; Abbott et al., 2014; Spencer et al., 2014; Vonk et al., 2015).

Approximately 10 L of water samples were collected from the northwestern inflowing river mouths and central Lake Taihu in March 2019 (see Fig. 2a for location of sampling sites) and they exhibited Chl-a

concentrations of 10.6 ± 3.6 and 10.0 ± 3.7, respectively (t-test, $p > 0.05$). Eighteen DOM samples from the northwestern inflowing river mouths and the central lake (2 sites × 3 time points × 3 replicates) were bio-incubated to determine how DON bio-lability in the two lake regions may influence the emission of N_2O. DOM samples with bacterial inoculum and nutrient amendment were bio-incubated following the aforementioned methods. An additional eighteen DOM samples (two sites × three time points × three replicates) with bacterial inoculum (2 mL site-specific GF/D filtrates for every 50 mL samples) and nutrient amendment (increased by 80 μM NH_4^+-N and 10 μM PO_4^{3-}-P) were poured into 61 mL brown glass bottles with excess sample material overflowing the bottles, and the samples were capped immediately without headspace using a butyl rubber stopper and sealed with an aluminum cap. High purity N_2 gas (99.999%) was injected into the bottles to create a 10 mL headspace, and the headspace of each vial was flushed with N_2 gas three times for 30 s prior to the bio-incubation. DON, DIN, DOC, DOM optical properties, and dissolved N_2O concentrations were measured on day 0, day 10, and day 20 following the above methods.

Eighteen additional DOM samples (2 sites × 3 time points × 3 replicates) collected from the northwestern inflowing river mouths and central Lake Taihu in March 2019 (see Fig. 2a for location of sampling sites) were photodegraded to unveil how DOM photo-degradability may influence the outgassing of N_2O. Filtrates passed through 0.22 μm Millipore filters with nutrient amendment only (increased by 80 μM NH_4^+-N and 10 μM PO_4^{3-}-P) were placed in ~100 mL quartz vials in an unshaded area and exposed to natural solar radiation. An additional eighteen DOM samples (two sites × three time points × three replicates) with nutrient amendment (increased by 80 μM NH_4^+-N and 10 μM PO_4^{3-}-P) were poured into 61 mL headspace quartz bottles with excess sample material overflowing the bottles. DON, DIN, DOC, and DOM optical properties and dissolved N_2O concentrations were measured on day 0, day 10, and day 20 following the aforementioned methods.

2.7. PARAFAC modeling and principal component analysis (PCA)

PARAFAC is a three-way statistical modeling approach that can decompose EEMs into non-co-varying components, aiding the characterization of the complex DOM pool (Stedmon et al., 2003), and thus be used to trace the linkage between DON optical composition and N_2O efflux. Samples collected during supplementary extensive sampling campaigns in October 2010 (n = 146), in January and June 2014, and in June 2015 (3 times × 113 sites) in the whole lake (see Fig. 1 for the location of sampling sites) were only included to facilitate PARAFAC modeling. PARAFAC modeling in this study was conducted with MATLAB R2015b using the drEEM version 0.2.0 toolbox (Murphy et al., 2013), and detailed information can be found in the Supporting Information. A six-component model was validated using split-half, random initialization and analysis of residuals (Stedmon and Bro, 2008; Murphy et al., 2013) and was found to adequately describe the whole EEMs data array (Fig. S2; Fig. S3).

PCA can be used to generate a reduced dataset explaining the majority of the variation of variables (Bro and Smilde, 2014). PCA was conducted on N_2O efflux, DIN, and DON-related indices, and some of the indices were later stepwise excluded from the model based on the correlation matrix and the associated significance level. Finally, 11 variables including N_2O efflux, Chl-a, COD, DON, DO, NO_3^--N, NH_4^+-N, a (350), $S_{275-295}$, and PARAFAC-derived C1 and C3 were included in the PCA modeling. The data array was preprocessed with autoscaling (mean centering followed by scaling where each column is divided by its standard deviation S.D.) prior to PCA (Bro and Smilde, 2014).

2.8. FT-ICR MS measurements and data processing

An increasing number of studies have applied electrospray ionization combined with ultra-high resolution Fourier transform ion
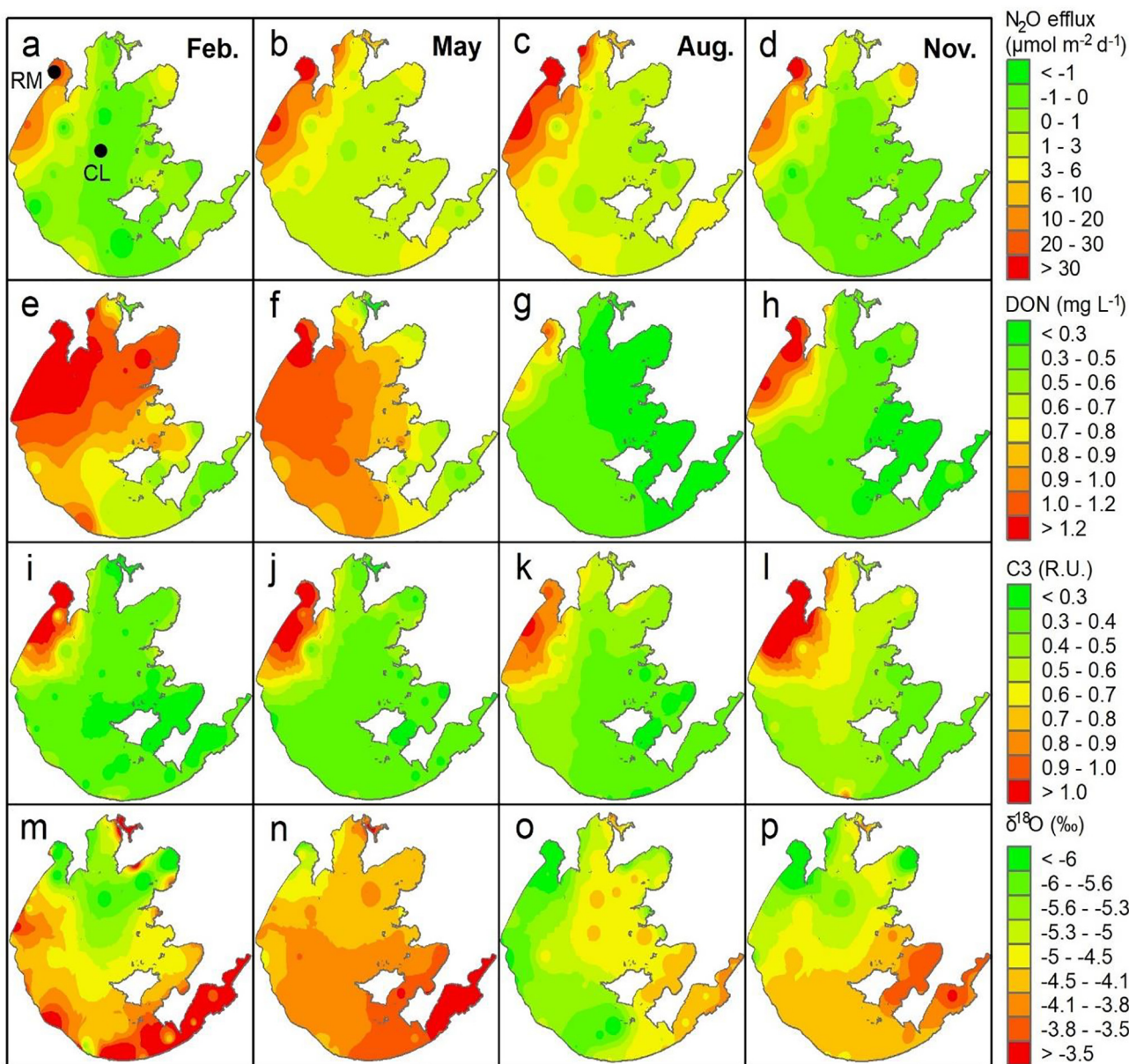
Fig. 2. Seasonal (February, May, August, and November) variability of multi-year (2012–2017) mean nitrous oxide (N_2O) efflux (a–d), dissolved organic nitrogen (DON, e–h), PARAFAC-derived terrestrial humic-like C3 (i–l), and stable isotopic $\delta^{18}O$-H_2O (m-p) in Lake Taihu. $\delta^{18}O$-H_2O data were only available for the lake water samples collected in 2012–2014. Locations of sample collection from the northwestern inflowing river mouths (RM) and the central lake (CL) for FT-ICR MS measurements and bio- and photo-degradation experiments are shown in panel a.

cyclotron resonance mass spectrometry (FT-ICR MS) to trace the compositional variability of DOM (Stubbins et al., 2012; Ohno et al., 2014; Spencer et al., 2014; Kellerman et al., 2015; Zhou et al., 2018b) and specifically DON (nitrogen-containing organic compounds) (Lusk and Toor, 2016a; Lusk and Toor, 2016b; Antony et al., 2017; Zhou et al., 2018c) at the molecular level in various aquatic ecosystems. A total of eleven samples, including six samples collected from the northwestern inflowing river mouths, the central lake (see Fig. 2a for location of sampling sites), and the southeastern outlet in November 2017 (n = 3) and November 2018 (n = 3), one sample in the central lake in August 2016, four samples from the northwestern inflowing river mouths and the central lake in August 2018 pre- (n = 2) and post- (n = 2) 28 days of bio-incubation, were solid-phase extracted using 6 mL PPL cartridges (Agilent) before the samples were analyzed using FT-ICR MS with negative-ion spray mode (Dittmar et al., 2008; Spencer et al., 2014).

Detailed information on the measurements and data processing can be found in the Supporting Information.

The assigned peaks were classified into seven categories: (i) lipids (O/C = 0–0.3, H/C = 1.5–2.0), (ii) proteins associated with amino acids (O/C = 0.3–0.67, H/C = 1.5–2.2), (iii) lignins (O/C = 0.1–0.67, H/C = 0.7–1.5), (iv) carbohydrates (O/C = 0.67–1.2, H/C = 1.5–2.2), (v) unsaturated hydrocarbons (O/C = 0–0.1, H/C = 0.7–1.5), (vi) condensed aromatics (O/C = 0–0.67, H/C = 0.2–0.7), and (vii) tannins (O/C = 0.67–1.2, H/C = 0.5–1.5) (Ohno et al., 2014; Zhou et al., 2018a). The aliphatic compounds are categorized as having <0.3 double bond equivalents (DBEs) per carbon atom and an H/C ratio ≥ 1 (Stubbins et al., 2010) or H/C ≥ 1.5, O/C < 0.9, N = 0 (Spencer et al., 2014). Spearman rank correlation coefficients were determined between the relative abundance of formulae assigned and the N_2O efflux in the corresponding lake regions using the in-built statistics toolbox in MATLAB R2015b.

2.9. Statistical analyses

Statistical analyses, including mean value, S.D., and *t*-test analyses, were performed with R i386 2.15.2. The location of sampling sites and spatial variability were mapped using ArcGIS 10.2 software. Linear, non-linear fittings, and PCA modeling were performed with the inbuilt statistics toolbox in MATLAB R2015b. Results of *t*-test and linear and nonlinear fittings with $p < 0.05$ were reported as significant.

3. Results

3.1. PARAFAC modeling results

The spectral characteristics of the six components were compared with those identified in other aquatic systems using an online fluorescence spectral library called OpenFluor (http://www.openfluor.org) (Murphy et al., 2014). C1 displayed two excitation maxima (at 235 and 305 nm), corresponding to a single emission maximum at 396 nm (Fig. S2; Fig. S3), and it was categorized as microbial humic-like substances (Stedmon and Markager, 2005; Kowalczuk et al., 2009; Murphy et al., 2011; Osburn et al., 2011; Kothawala et al., 2014). C2 (Ex/Em ≤ 230 (285)/340 nm) and C5 (Ex/Em = 275/348 nm) (Fig. S2; Fig. S3) were characterized as representing tryptophan-like substances associating closely with amino acids (Stedmon and Markager, 2005; Murphy et al., 2011; Catala et al., 2015; Wünsch et al., 2017). These two components may originate from the moieties of polyphenols (Hur et al., 2011) or the degradation of algae cells (Zhang et al., 2009; Zhou et al., 2018a). C3 (Ex/Em = 235 (355)/468 nm) exhibited spectral shapes (Fig. S2; Fig. S3) that represented terrestrial organic-rich substances (Kowalczuk et al., 2009; Williams et al., 2010; Stedmon et al., 2011; Kowalczuk et al., 2013; Catala et al., 2015). C4 (Ex/Em ≤ 230 (275)/316 nm) and C6 (Ex/Em ≤ 230 (275)/300 nm) had spectral shapes (Fig. S2; Fig. S3) similar to red-shifted tyrosine-like and typical tyrosine-like substances, respectively (Stedmon and Markager, 2005; Walker et al., 2009; Murphy et al., 2011; Kowalczuk et al., 2013).

3.2. General characteristics of N₂O efflux and DOM-related variables

Urban land cover (%cities) of the five sub-watersheds Huxi, Zhexi, Wuchengxiyu, Hangjiahu, and Yangchengdianmao in 2015 was 17%, 5%, 35%, 25%, and 29%, respectively (Fig. 1). The N₂O efflux in Lake Taihu during 2012–2017 ranged between −7.1 and 195 μmol m⁻² d⁻¹ with a mean of 5.0 ± 17.6 μmol m⁻² d⁻¹, and the multi-year mean N₂O efflux was significantly higher in May and August than in February and November (Paired *t*-test, $p < 0.01$) (Fig. 2; Table S1; Table S2). The multi-year mean N₂O efflux was significantly higher in lake regions connected to the northwestern inflowing sub-watershed Huxi than in the remaining lake regions (*t*-test, $p < 0.001$; Table S1; Table S3). DON concentrations ranged between 0.01 and 2.78 mg L⁻¹ (Fig. 2), constituting 43.0 ± 33.1% of TDN in the lake in all seasons. N₂O efflux, DON, COD, bacterial abundance, Chl-*a*, DOC, NO₃⁻-N, NH₄⁺-N, NO₂⁻-N, *a*(350), SUVA₂₅₄, I_C:I_T, and C1-C4 and C6 decreased markedly in all seasons from the northwestern inflowing river mouths to the southeastern bays (Fig. 2; Figs. S4–S6; Table S3). Enriched δ¹⁵N-TDN (>6‰) and depleted δ¹³C-DOC (<−26.5‰) were found in the northwestern inflowing river mouths with correspondingly high DON concentrations (Figs. S7–S8). High levels of Chl-*a* were recorded in the northern half of the lake, especially in the northern Meiliang Bay but not in the northwestern inflowing Zhushan Bay (Fig. S4; Fig. S6). In comparison, δ¹⁸O, DO, and S₂₇₅₋₂₉₅ all increased from the northwestern inflowing river mouths to the southeastern outflowing bays in the lake in all seasons (Fig. 2; Fig. S4; Fig. S6; Table S3).

As high levels of DON and N₂O efflux are found in the northwestern inflowing river mouths (Fig. 2; Fig. S4; Table S3) and as terrestrial humic-like components can be highly photochemically labile, the spatial variability of C3 and light penetration in the northwestern lake area with large inflows was further investigated. We found high levels of C3 discharged and accumulated in the northwestern lake region with large inflows in all seasons (Fig. 2) and low levels of K_d(305) and K_d(340), i.e. strong downwelling irradiance in the underwater light climate in the northwestern inflowing river mouths (Fig. S7).
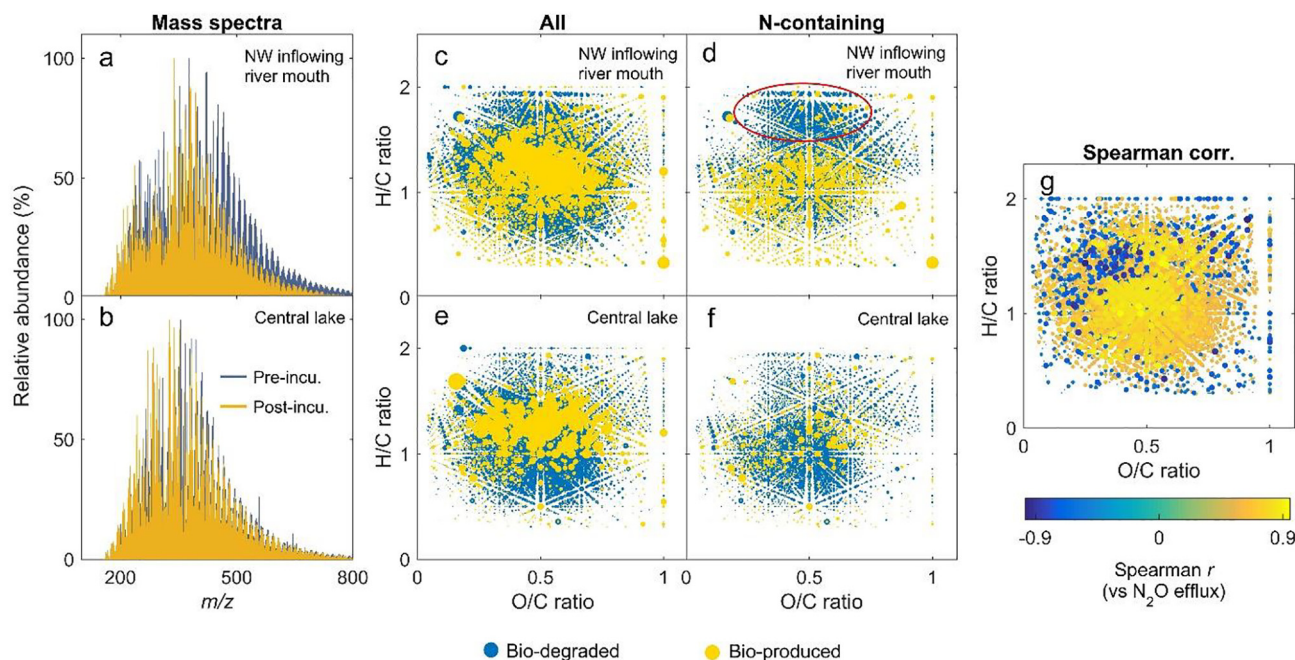

Fig. 3. Ultra-high resolution FT-ICR MS spectra over the *m/z* range 150–800 for the samples collected in the northwestern (NW) inflowing river mouths and the central part of Lake Taihu (see Fig. 2a) pre- and post-28 days of bio-incubation (a–b). van Krevelen diagrams showing the O/C vs H/C ratio of all formulae and the N-containing molecular formulae for the two samples as biodegraded or bio-produced after 28 days of bio-incubation (c–f). The sizes of the dot are proportional to the bio-degraded or bio-produced relative abundance of the FT-ICR MS-identified molecules in panels c–f. (g) shows Spearman correlation coefficients between the relative abundances of FT-ICR MS-identified molecules and the mean N₂O efflux in the corresponding lake regions with |r| > 0.4 and $p < 0.05$.

3.3. FT-ICR MS results

We selected samples collected from the northwestern inflowing river mouths and the central lake (n = 4, two for pre- and two for post-incubation) in August 2018 to investigate how 28 days of bio-incubation changed the molecular signature of DOM in different regions of the lake (Fig. 3; Tables S4–S6). CHON-containing formulae for the samples collected from the northwestern inflowing river mouths and the central lake pre- and post-28 days of bio-incubation accounted for 33.6%, 33.9% and 34.4%, 34.7% of the formulae and, correspondingly, 29.6%, 34.0% and 33.3%, 33.7% of the intensity of all formulae, respectively (Tables S4–S6). The relative intensity distribution for the northwestern inflowing river mouths and the central lake DOM samples centered around m/z 400 and m/z 350, respectively (Fig. 3). The aliphatic peaks of the samples collected from the northwestern inflowing river mouths and the central lake pre- and post-28 days of bio-incubation changed from 13%, 14% to 12%, 14% of the formulae and, correspondingly, from 11%, 13% to 12%, 14% of the relative abundance, respectively (Fig. 3; Table S4).

The 28 days of bio-incubation decreased the average molecular weight of solid-phase extracted DOM collected from the northwestern inflowing river mouths, leading to the change of the bell-like relative intensity distribution centered from around m/z 400 to m/z 350 (Fig. 3a). The mass spectra of the DOM sample collected from the central lake with relative intensity distribution decreased insignificantly after the 28 days of bio-incubation (Fig. 3b). The molecular weight decrease after the 28 days of bio-incubation resulted in reduced relative abundance of aliphatic peaks for all formulae, this being especially pronounced for the N-containing formulae assigned to the DOM sample collected from the northwestern inflowing river mouths (Fig. 3c–f).

A total of 6459 formulae were correlated with the N_2O efflux with an absolute Spearman correlation coefficient $|r| \geq 0.4$ and $p < 0.05$ (Fig. 3g). The relative abundance of 4853 formulae, mostly terrestrial lignin compounds, increased notably, while the remaining 1606 formulae, mostly aliphatic molecules (including lipids and proteins), decreased with increasing N_2O effluxes (Fig. 3g).

3.4. Relationships between N_2O efflux, DON, DIN, and DOM-related variables

We found significant positive relationships between the logarithm-transformed N_2O efflux, i.e. $\log_{10}(N_2O + |N_2O_{min}| + 1)$ ($N_2O_{min} = -7.1$ μmol m^{-2} d^{-1}), and DON, DON × net inflow, Chl-a, DOC, SUVA$_{254}$, and terrestrial humic-rich C3 ($p < 0.01$) (Fig. 4), bacterial abundance, COD, $a(350)$, and microbial humic-like C1 ($p < 0.001$) (Fig. S8). Significant negative relationships were recorded between the logarithm-transformed N_2O efflux and DO, $\delta^{18}O$, and $S_{275-295}$ ($p < 0.001$) (Fig. 4; Fig. S9). No significant relationship was observed between the N_2O efflux and PARAFAC-derived C2 and C4-C6 (Fig. S9).

We found that the logarithm-transformed N_2O efflux correlated positively with NH_4^+-N, NO_3^--N, and NO_2^--N ($p < 0.001$) in Lake Taihu during 2012–2017 (Fig. S1). Significant positive relationships were observed between DON and DOC ($p < 0.05$), $a(350)$, SUVA$_{254}$, and PARAFAC-derived C3 and C4 ($p < 0.01$) (Table S7). We found significant negative relationships between DON and $\delta^{18}O$, $S_{275-295}$ ($p < 0.01$) (Table S7). No significant relationship was detected between DON and COD, DO, Chl-a, or PARAFAC-derived C1-C2 or C5-C6 (Table S7). Significant positive relationships were discovered between NH_4^+-N and a (350), terrestrial humic-rich C3, DON, and DOC ($p < 0.001$) and negative relationship between NH_4^+-N and $\delta^{18}O$, $S_{275-295}$ ($p < 0.001$) (Fig. 5;
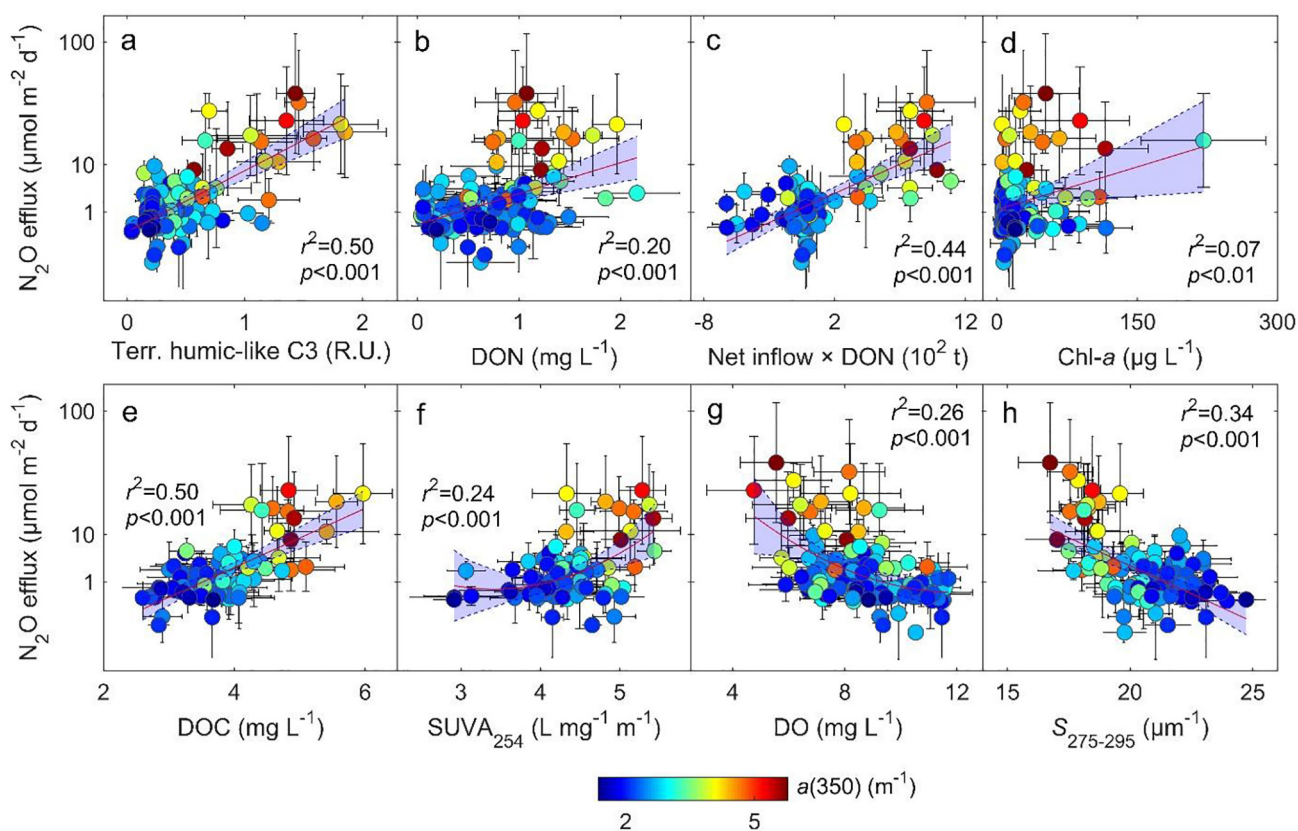

Fig. 4. Relationships between the logarithm-transformed N_2O efflux, i.e. $\log_{10}(N_2O + |N_2O_{min}| + 1)$ ($N_2O_{min} = -7.1$ μmol m^{-2} d^{-1}), and terrestrial humic-like C3 (a), dissolved organic nitrogen (DON, b), products of net inflow discharge and DON (c), chlorophyll-a (Chl-a, d), dissolved organic carbon (e), specific ultraviolet absorbance (SUVA$_{254}$, f), dissolved oxygen (DO, g), and spectral slope of CDOM absorption $S_{275-295}$ (h) for the samples collected seasonally from the five lake regions in Lake Taihu. Data on net inflow discharge were only available for 2012–2016 and data on DOC and SUVA$_{254}$ were only available for the samples collected since May 2013. Error bars in all panels represent ±1 SD of samples collected from the different lake regions shown in Fig. 1.
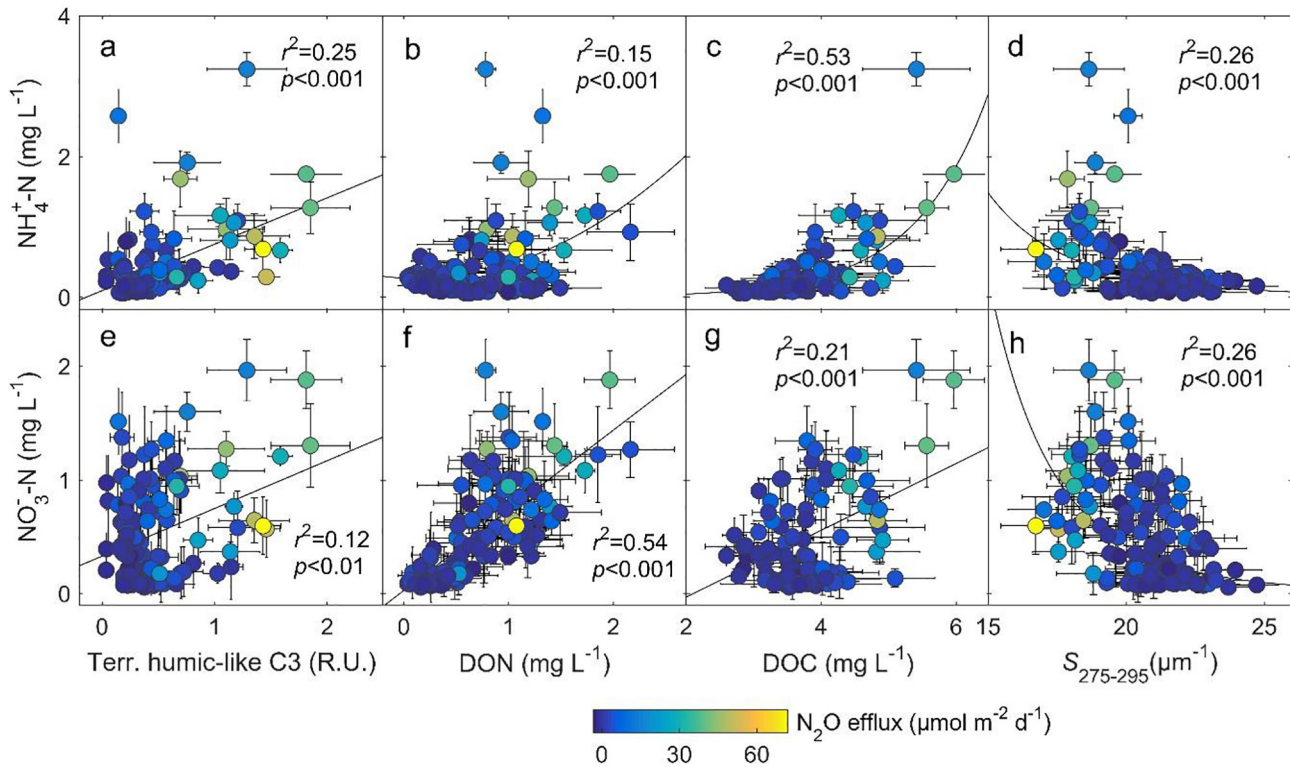
Fig. 5. Relationships between NH_4^+-N and terrestrial humic-like C3 (a), dissolved organic nitrogen (DON, b), dissolved organic carbon (DOC, c), spectral slope of CDOM absorption $S_{275-295}$ (d). Relationships between NO_3^--N and terrestrial humic-like C3 (e), dissolved organic nitrogen (DON, f), dissolved organic carbon (DOC, g), spectral slope of CDOM absorption $S_{275-295}$ (h) for the samples collected seasonally from the five lake regions in Lake Taihu. Error bars in all panels represent ± 1 SD of samples collected from the different lake regions shown in Fig. 1.

Table S7). We further found that NO_3^--N and NO_2^--N concentrations increased with increasing $a(350)$, terrestrial humic-rich C3, DON, and DOC ($p < 0.001$) and with decreasing $\delta^{18}O$, $S_{275-295}$ ($p < 0.001$) (Fig. 5; Table S7).

In the PCA analysis, the first two components, i.e. PC1 and PC2, explained 47.3% and 18.4%, respectively, of the variability of the 11 variables included. N_2O efflux, Chl-a, COD, DON, NO_3^--N, NH_4^+-N, $a(350)$, and PARAFAC-derived C1 and C3 displayed positive PC1 loadings, while DO and $S_{275-295}$ demonstrated negative PC1 loadings (Fig. 6),

implying that PC1 is positively related to the terrestrial DON input and the N_2O efflux. NO_3^--N showed high PC2 loadings (Fig. 6), suggesting that PC2 may be positively related to the NO_3^--N input.

3.5. Bio- and photo-degradation results of the headspace samples

The inflowing water CDOM sample exhibits strong terrestrial organic-rich signals compared with the central Lake Taihu sample. The initial mean $a(250){:}a(365)$ and $S_{275-295}$ for the samples collected from
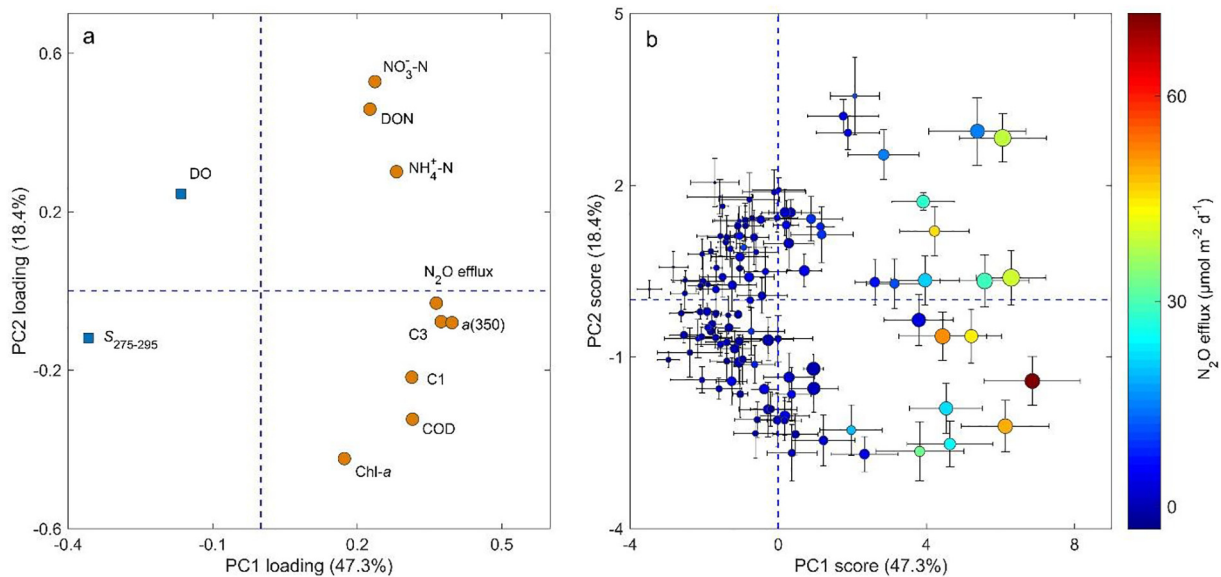

Fig. 6. PCA factor loadings (left) and scores (right) for the samples collected from Lake Taihu seasonally from 2012 to 2017. The size of the dots shown in the right panel is proportional to the F_{max} of terrestrial humic-rich C3, and the color of the dots represents the N_2O efflux. Error bars in the right panel represent ± 1 SD of samples collected from the different lake regions shown in Fig. 1.

the northwestern inflowing river mouths were significantly lower than in the samples from the central lake sites (*t*-test, $p < 0.001$) (Fig. S10). SUVA$_{254}$ for the northwestern inflowing river mouths samples was significantly higher than for the central lake samples (*t*-test, $p < 0.001$) (Fig. S10).

In the bio-degradation experiment, dissolved N$_2$O concentrations increased significantly (1369% increase, *t*-test, $p < 0.001$ and 281% increase, *t*-test, $p < 0.001$) during the 20 days of bio-incubation for the samples collected from the northwestern inflowing river mouths and the central lake, respectively (Fig. 7). For the sample collected from the northwestern inflowing river mouths, DON, DOC, $a(254)$, NH$_4^+$-N, and F$_{max}$ of C2-C5 decreased during the 20 days of bio-incubation (*t*-test, $p < 0.001$, Fig. 7; Fig. S11). NO$_3^-$-N increased on day 10 and decreased on day 20, NO$_2^-$-N increased (*t*-test, $p < 0.001$), and no significant difference was found between the means of the F$_{max}$ of C1 and C6 during the 20 days of bio-incubation (Fig. 7; Fig. S11). For the samples collected from the central lake, $a(254)$, NH$_4^+$-N, and NO$_3^-$-N and the F$_{max}$ of C2 decreased during the 20 days of bio-incubation (*t*-test, $p < 0.001$, Fig. 7; Fig. S11). DON, DOC, and NO$_2^-$-N increased (*t*-test, $p < 0.001$), while no significant difference was found between the means of the F$_{max}$ of C1 and C3-C6 during the 20 days of bio-incubation (Fig. 7; Fig. S11).

For the photo-degradation experiment, dissolved N$_2$O increased (195% increase, *t*-test, $p < 0.001$ and 171% increase, *t*-test, $p < 0.001$) after 20 days of photo-degradation for the samples collected from the northwestern inflowing river mouths and the central lake, respectively (Fig. 7). For the sample collected from the northwestern inflowing river mouths, $a(254)$, NH$_4^+$-N, NO$_3^-$-N, and NO$_2^-$-N and the F$_{max}$ of C1-C5 decreased notably during the 20 days of photo-degradation (*t*-test, $p < 0.001$, Fig. 7; Fig. S11). DON and DOC decreased on day 10 and increased notably on day 20, and the F$_{max}$ of C6 increased (*t*-test, $p < 0.001$) after the 20 days of photo-degradation (Fig. 7; Fig. S11). For the samples collected from the central lake, $a(254)$, NH$_4^+$-N, and NO$_3^-$-N and the F$_{max}$ of C1-C5 decreased during the 20 days of photo-degradation (*t*-test, $p < 0.001$, Fig. 7; Fig. S11). DON, DOC, and NO$_2^-$-N and the F$_{max}$ of C6 increased after the 20 days of photo-degradation (*t*-test, $p < 0.001$, Fig. 7; Fig. S11).

4. Discussion

4.1. N$_2$O efflux indirectly fueled by DON input

Our results collectively indicate that the terrestrial DON and DOC input and the subsequent degradation in the northwestern inflowing river mouths fueled ammonification and oxygen depletion, thereby enhancing incomplete aerobic nitrification and nitrifier denitrification, which in turn increased the N$_2$O efflux from Lake Taihu.

Field observations found high N$_2$O efflux across all seasons in the inflow-affected northwestern areas and the accumulation and subsequent degradation of terrestrial DON and DOC here (Fig. 2; Figs. 4–5; Fig. S4) probably served as terminal electron donors for nitrification and denitrification. This is supported by the fact that most of the N$_2$O efflux variation could be explained by terrestrial humic-rich C3, DOC input, $a(350)$, and net inflow × DON (Fig. 4), and by the fact that in the PCA results the N$_2$O efflux was also closely associated with the terrestrial DON input (Fig. 6). The close relationships revealed between terrestrial humic-rich lignin compounds by FT-ICR MS and the N$_2$O efflux with an absolute Spearman correlation coefficient $|r| \geq 0.4$ and $p < 0.05$ (Fig. 3) provided further evidence of this. DON is the concentration of the organic fraction of nitrogen, whilst net inflow × DON directly
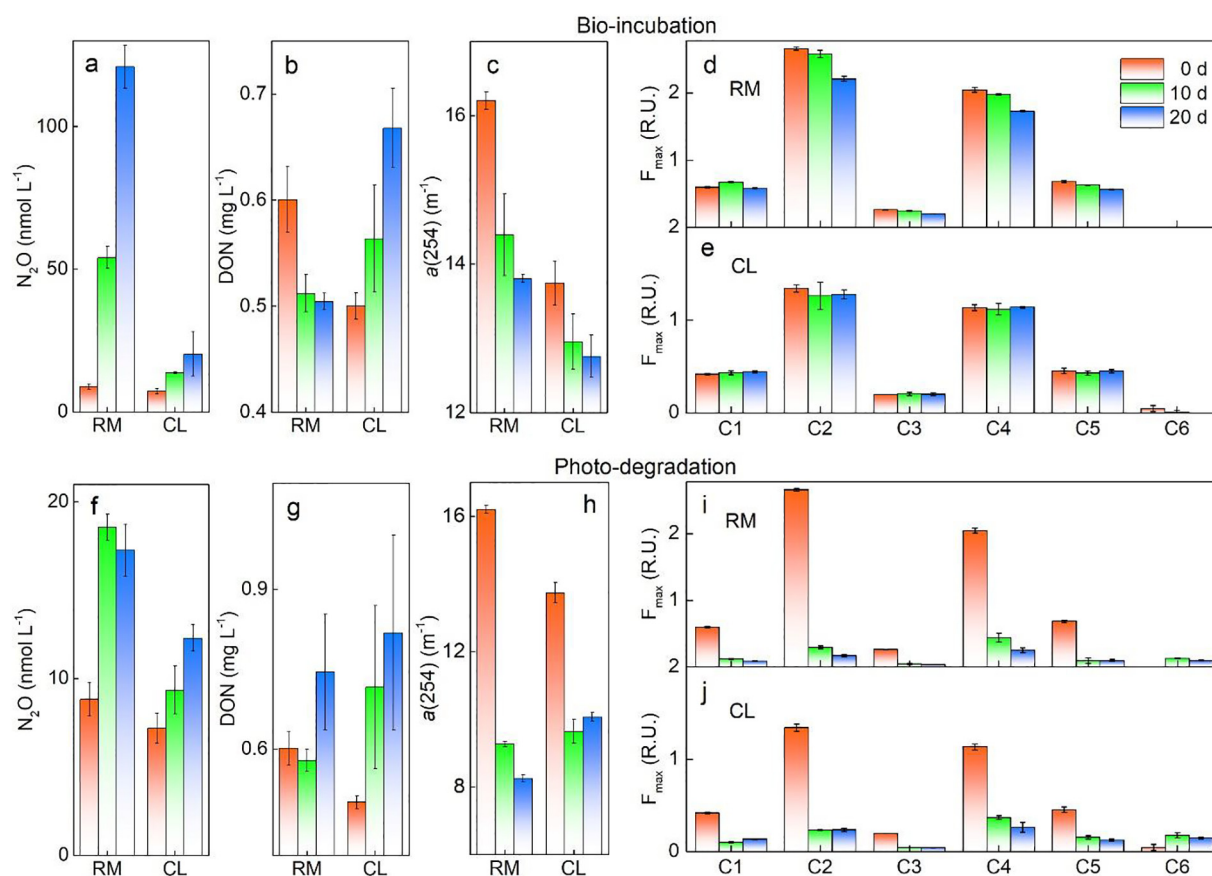

Fig. 7. Dissolved N$_2$O concentrations, dissolved organic nitrogen (DON), CDOM absorption $a(254)$, and fluorescence intensity (F$_{max}$) of the six PARAFAC components C1-C6 on day 0, day 10, and day 20 for the bio-incubated samples collected from the northwestern inflowing river mouths (RM) and in central Lake Taihu (CL) (a–e, see Fig. 2a). N$_2$O, DON, $a(254)$, and F$_{max}$ of C1-C6 on day 0, day 10, and day 20 for the photo-degraded samples collected from RM and CL (f–j). Error bars in all panels represent ±1 S.D. of triplicate samples.

represents the load of DON to the lake, the latter explained a large part of the variation in the N_2O efflux from the lake (Fig. 4). The stronger relationships between the N_2O efflux and NH_4^+-N than between the N_2O efflux and NO_3^--N (Fig. S1) suggest that nitrification and nitrifier denitrification contributed more importantly to the N_2O efflux from the lake than did denitrification of NO_3^--N, a finding that is consistent with previous results obtained from other ecosystems (Beaulieu et al., 2010; Yu et al., 2013). The large and highly polluted inflow discharge in the northwestern inflowing area (Qin et al., 2007) favor degradation of the labile DON and DOC accumulated here, thereby elevating ammonification as well as DO consumption. This is supported by the positive relationships between NH_4^+-N and DON, DOC, $a(350)$, and terrestrial humic-rich C3 (Fig. 5) and the low DO in the inflow river mouths (Fig. S6). DO depletion may increase the incomplete aerobic nitrification in the water columns (Fig. 8). Nitrifier denitrification (NH_4^+-N → NO_2^--N → N_2O → N_2), a pathway of nitrification, may also have contributed to the enhanced N_2O efflux at high NH_4^+-N and low DO concentrations (Fig. 8; Figs. S5–S6). Previous studies have shown incomplete aerobic nitrification and nitrifier denitrification to be kinetically favorable when DO <5 mg L^{-1} (Cébron et al., 2005; Yu et al., 2013). Moreover, high NO_3^--N concentrations (Fig. S5) in the northwestern inflowing area potentially enhance denitrification and, if incomplete, also the N_2O efflux from the sediment. The weak relationships recorded between the N_2O efflux and Chl-a, autochthonous protein-like C2, C4-C6 for all samples and for the samples collected in summer (Fig. 4; Fig. S9; Fig. S12) suggest that algal degradation was not the primary driver of the N_2O efflux from the lake.

Laboratory experiments showed that both bio- and photodegradation resulted in a more pronounced increase in N_2O in the northwest inflow areas than in the central lake (Fig. 7). Samples collected from the river inflow-affected areas in the northwestern and central parts of lake both had low Chl-a values, but the lower $a(250){:}a(365)$ and $S_{275-295}$ and higher $SUVA_{254}$ in the inflow-affected area (Fig. S10) in the northwest indicate a strong terrestrial humic-rich influence here compared with the central lake. Enhanced ammonification and thereafter nitrification or nitrifier denitrification occurred as indicated by the rapid consumption of DON, DOC, and $a(254)$, and decreased NH_4^+-N and NO_3^--N during the 20 days of bio-incubation, especially in the northwest inflow lake water samples (Fig. 7; Fig. S11). The enhanced nitrification in the northwest inflow lake water samples can be explained by the decrease in NH_4^+-N (Fig. 7; Fig. S11). The consumption of PARAFAC-derived C2-C5 for samples collected in the northwest areas with large inflow further underlines the importance of terrestrial

DON, as electron donors for nitrification here. C3 is a typical terrestrial component that is closely associated with riverine soil organic-rich compounds (Coble, 2007; Stedmon et al., 2007; Hur et al., 2014; Williams et al., 2016; Murphy et al., 2018; Song et al., 2018).

4.2. DON sources and lability

That DON accumulated in the inflow-affected area in the northwest was most likely of riverine origin is supported by the high levels of $SUVA_{254}$ and $I_C{:}I_T$, and the low levels of $S_{275-295}$ (Fig. 2; Fig. S4; Fig. S6). $SUVA_{254}$ and $I_C{:}I_T$ have been shown to increase with increasing terrestrial DOM aromaticity (Weishaar et al., 2003; Spencer et al., 2014; Zhou et al., 2017). $S_{275-295}$ has been widely shown to decrease with increasing DOM aromaticity (Fichot and Benner, 2012; Shen et al., 2012). Enriched δ^{15}N-DTN, depleted δ^{13}C-DOC and δ^{18}O, and high COD (Fig. S4; Figs. S7–S8) in the northwestern region indicate a substantial input of anthropogenic effluents and terrestrial organic-rich substances into Lake Taihu from the terrestrial environment and household and agricultural sewage (Vizzini et al., 2005; Zhou et al., 2018c). Riverine δ^{18}O with short residence time usually exhibits depleted signatures (Wu et al., 2015; Xiao et al., 2016; Zhou et al., 2018b). DON is the N-containing fraction of DOM and its variability is closely associated with its carbon skeleton in various environments (Lusk and Toor, 2016b; Lusk and Toor, 2016a; Osburn et al., 2016; Hounshell et al., 2017). The northwestern inflowing river mouths host a large range of microorganisms in high abundances (Fig. S6), and DON might be closely linked to the microbial release of amino acids (Stedmon et al., 2011; Xu et al., 2013; Tang et al., 2017). Recent studies further showed that the net inflow discharge to the lake primarily occurs in the northwest, in particular the Huxi (Fig. 1) river mouths (Qin et al., 2007; Zhou et al., 2018b; Zhou et al., 2018c). This is further supported by the higher relative intensity distribution for the northwestern inflowing river mouths (centered m/z 400) relative to the central lake DOM samples (m/z 350) (Fig. 3) and the high percentage contributions of lignins, tannins, and condensed aromatic molecular formulae assigned to the samples collected from the northwestern area with large inflow (Fig. 3; Tables S4–S6). Lignins, tannins, and aromatic substances are widely considered to be vascular plant-derived polyphenols (Stubbins et al., 2010) that prevail in the lake (Zhou et al., 2018b).

A fraction of DON accumulated in the northwestern areas with the largest inflows is highly labile. The rapid degradation of N-binding aliphatic molecules with H/C > 1.5 and the shift in the bell-like relative intensity distribution centered from around m/z 400 to m/z 350 of the
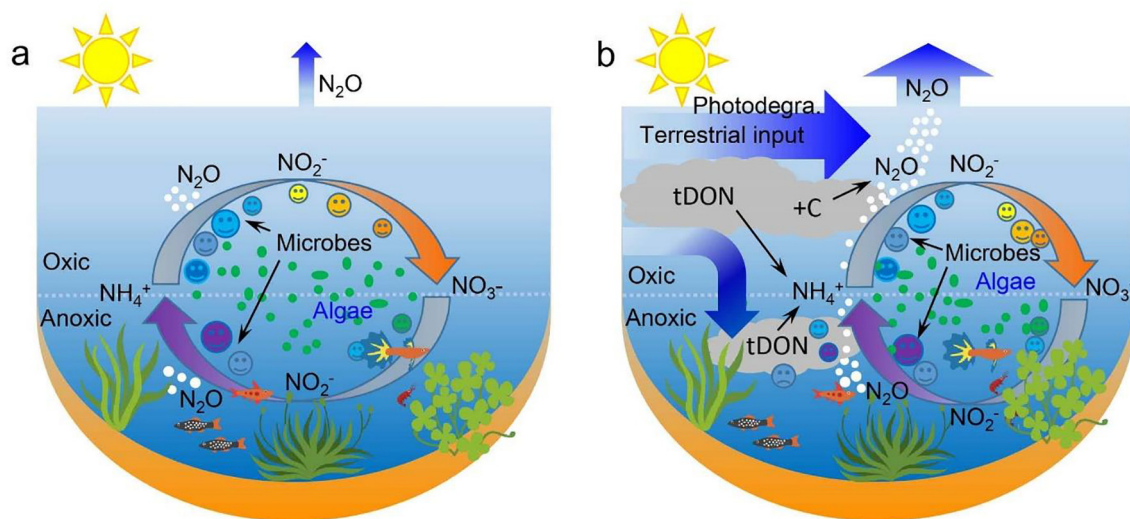

Fig. 8. Conceptual diagram illustrating the potential factors affecting the N_2O efflux from the shallow lakes without (a) and with (b) strong terrestrial DON (tDON) input and the subsequent accumulation and processing in the inflowing river mouths of Lake Taihu.

river mouth sample revealed by FT-ICR MS during the 28 days of bio-incubation provided evidence of this (Fig. 3; Table S5). Low diffuse attenuation coefficients of light at UV-B and UV-A, i.e. $K_d(305)$ and $K_d(340)$, in the northwestern inflowing river mouths (Fig. S7), indicating high UV light availability of the underwater light climate, also point to a higher photochemical degradation potential and thereby potentially enhanced ammonification here than in the main lake. Our results therefore suggest that a reduction of the external DON loading (i.e. improved wastewater treatment capability in the upstream northwestern sub-watershed) could help to reduce the N_2O efflux from the eutrophic Lake Taihu.

4.3. Implications

Current models have failed to capture the underlying factors affecting the dynamic nature of the N_2O efflux in N-rich waters with a strong terrestrial DON input (Soued et al., 2015). The variability and the underlying drivers need to be revealed if we are to improve our knowledge of the global N_2O budget (Jetten, 2008). In our study, no information was available on the composition of sediment pore water DON, which is an important source of N_2O (Kuypers et al., 2018), and the linkage between labile DON in sediment pore water and the N_2O efflux from lakes deserves further investigations.

CRediT authorship contribution statement

Yongqiang Zhou: Conceptualization, Writing - original draft, Writing - review & editing, Funding acquisition. **Qitao Xiao:** Methodology, Investigation, Data curation, Methodology. **Lei Zhou:** Data curation, Investigation, Writing - review & editing. **Kyoung-Soon Jang:** Data curation, Software, Writing - review & editing. **Yunlin Zhang:** Funding acquisition, Resources, Supervision. **Mi Zhang:** Data curation, Investigation. **Xuhui Lee:** Data curation, Investigation. **Boqiang Qin:** Funding acquisition, Resources, Supervision. **Justin D. Brookes:** Writing - review & editing. **Thomas A. Davidson:** Writing - review & editing. **Erik Jeppesen:** Writing - review & editing.

Declaration of competing interest

The authors declare that they have no known competing financial interests or personal relationships that could have appeared to influence the work reported in this paper.

Appendix A. Supplementary data

Supplementary data to this article can be found online at https://doi.org/10.1016/j.scitotenv.2020.138005.

References

Abbott, B.W., Larouche, J.R., Jones, J.B., Bowden, W.B., Balser, A.W., 2014. Elevated dissolved organic carbon biodegradability from thawing and collapsing permafrost. J. Geophys. Res. Biogeosci. 119, 2049–2063.

Aben, R.C.H., Barros, N., van Donk, E., Frenken, T., Hilt, S., Kazanjian, G., et al., 2017. Cross continental increase in methane ebullition under climate change. Nat. Commun. 8, 1682. https://doi.org/10.1038/s41467-017-01535-y.

Antony, R., Willoughby, A.S., Grannas, A.M., Catanzano, V., Sleighter, R.L., Thamban, M., et al., 2017. Molecular insights on dissolved organic matter transformation by supraglacial microbial communities. Environ. Sci. Technol. 51, 4328–4337. https://doi.org/10.1021/acs.est.6b05780.

Beaulieu, J., Shuster, W., Rebholz, J., 2010. Nitrous oxide emissions from a large, impounded river: the Ohio River. Environ. Sci. Technol. 44, 7527–7533.

Beaulieu, J.J., Tank, J.L., Hamilton, S.K., Wollheim, W.M., Hall, R.O., Mulholland, P.J., et al., 2011. Nitrous oxide emission from denitrification in stream and river networks. Proc. Natl. Acad. Sci. U. S. A. 108, 214–219.

Bro, R., Smilde, A.K., 2014. Principal component analysis. Anal. Methods 6, 2812–2831. https://doi.org/10.1039/c3ay41907j.

Catala, T.S., Reche, I., Fuentes-Lema, A., Romera-Castillo, C., Nieto-Cid, M., Ortega-Retuerta, E., et al., 2015. Turnover time of fluorescent dissolved organic matter in the dark global ocean. Nat. Commun. 6, 5986. https://doi.org/10.1038/ncomms6986.

Cébron, A., Garnier, J., Billen, G., 2005. Nitrous oxide production and nitrification kinetics by natural bacterial communities of the lower Seine river (France). Aquat. Microb. Ecol. 41, 25–38.

Coble, P.G., 2007. Marine optical biogeochemistry: the chemistry of ocean color. Chem. Rev. 107, 402–418. https://doi.org/10.1021/cr050350+.

Davidson, E.A., 2009. The contribution of manure and fertilizer nitrogen to atmospheric nitrous oxide since 1860. Nat. Geosci. 2, 659–662.

Davidson, T.A., Audet, J., Svenning, J.C., Lauridsen, T.L., Sondergaard, M., Landkildehus, F., et al., 2015. Eutrophication effects on greenhouse gas fluxes from shallow-lake mesocosms override those of climate warming. Glob. Chang. Biol. 21, 4449–4463. https://doi.org/10.1111/gcb.13062.

Davidson, T.A., Audet, J., Jeppesen, E., Landkildehus, F., Lauridsen, T.L., Søndergaard, M., et al., 2018. Synergy between nutrients and warming enhances methane ebullition from experimental lakes. Nat. Clim. Chang. 8, 156–160. https://doi.org/10.1038/s41558-017-0063-z.

Dittmar, T., Koch, B., Hertkorn, N., Kattner, G., 2008. A simple and efficient method for the solid-phase extraction of dissolved organic matter (SPE-DOM) from seawater. Limnol. Oceanogr. Methods 6, 230–235.

Elberling, B., Christiansen, H.H., Hansen, B.U., 2010. High nitrous oxide production from thawing permafrost. Nat. Geosci. 3, 332–335. https://doi.org/10.1038/ngeo803.

Fichot, C.G., Benner, R., 2012. The spectral slope coefficient of chromophoric dissolved organic matter (S275-295) as a tracer of terrigenous dissolved organic carbon in river-influenced ocean margins. Limnol. Oceanogr. 57, 1453–1466. https://doi.org/10.4319/lo.2012.57.5.1453.

Griffis, T.J., Chen, Z., Baker, J.M., Wood, J.D., Millet, D.B., Lee, X., et al., 2017. Nitrous oxide emissions are enhanced in a warmer and wetter world. Proceedings of the National Academy of Science of the United State of America 114, 12081–12085. https://doi.org/10.1073/pnas.1704552114.

Guo, W., Yang, L., Zhai, W., Chen, W., Osburn, C.L., Huang, X., et al., 2014. Runoff-mediated seasonal oscillation in the dynamics of dissolved organic matter in different branches of a large bifurcated estuary-the Changjiang Estuary. J. Geophys. Res. Biogeosci. 119, 776–793. https://doi.org/10.1002/2013jg002540.

Heinz, M., Graeber, D., Zak, D., Zwirnmann, E., Gelbrecht, J., Pusch, M.T., 2015. Comparison of organic matter composition in agricultural versus forest affected headwaters with special emphasis on organic nitrogen. Environ. Sci. Technol. 49, 2081–2090. https://doi.org/10.1021/es505146h.

Helms, J.R., Stubbins, A., Ritchie, J.D., Minor, E.C., Kieber, D.J., Mopper, K., 2008. Absorption spectral slopes and slope ratios as indicators of molecular weight, source, and photobleaching of chromophoric dissolved organic matter. Limnol. Oceanogr. 53, 955–969.

Hood, E., Fellman, J., Spencer, R.G., Hernes, P.J., Edwards, R., D'Amore, D., et al., 2009. Glaciers as a source of ancient and labile organic matter to the marine environment. Nature 462, 1044–1047. https://doi.org/10.1038/nature08580.

Hounshell, A.G., Peierls, B.L., Osburn, C.L., Paerl, H.W., 2017. Stimulation of phytoplankton production by anthropogenic dissolved organic nitrogen in a coastal plain estuary. Environ. Sci. Technol. 51, 13104–13112. https://doi.org/10.1021/acs.est.7b03538.

Hu, M., Chen, D., Dahlgren, R.A., 2016. Modeling nitrous oxide emission from rivers: a global assessment. Glob. Chang. Biol. 22, 3566–3582.

Huang, C., Jiang, Q., Yao, L., Yang, H., Lin, C., Huang, T., et al., 2018. Variation pattern of particulate organic carbon and nitrogen in oceans and inland waters. Biogeosciences 15, 1827–1841. https://doi.org/10.5194/bg-15-1827-2018.

Hur, J., Jung, K.Y., Schlautman, M.A., 2011. Altering the characteristics of a leaf litter-derived humic substance by adsorptive fractionation versus simulated solar irradiation. Water Res. 45, 6217–6226. https://doi.org/10.1016/j.watres.2011.09.023.

Hur, J., Lee, B.-M., Lee, S., Shin, J.-K., 2014. Characterization of chromophoric dissolved organic matter and trihalomethane formation potential in a recently constructed reservoir and the surrounding areas – impoundment effects. J. Hydrol. 515, 71–80. https://doi.org/10.1016/j.jhydrol.2014.04.035.

Jetten, M.S.M., 2008. The microbial nitrogen cycle. Environ. Microbiol. 10, 2903–2909. https://doi.org/10.1111/j.1462-2920.2008.01786.x.

Kellerman, A.M., Kothawala, D.N., Dittmar, T., Tranvik, L.J., 2015. Persistence of dissolved organic matter in lakes related to its molecular characteristics. Nat. Geosci. 8, 454–457. https://doi.org/10.1038/ngeo2440.

Kothawala, D.N., Stedmon, C.A., Muller, R.A., Weyhenmeyer, G.A., Kohler, S.J., Tranvik, L.J., 2014. Controls of dissolved organic matter quality: evidence from a large-scale boreal lake survey. Glob. Chang. Biol. 20, 1101–1114. https://doi.org/10.1111/gcb.12488.

Kowalczuk, P., Durako, M.J., Young, H., Kahn, A.E., Cooper, W.J., Gonsior, M., 2009. Characterization of dissolved organic matter fluorescence in the South Atlantic Bight with use of PARAFAC model: interannual variability. Mar. Chem. 113, 182–196. https://doi.org/10.1016/j.marchem.2009.01.015.

Kowalczuk, P., Tilstone, G.H., Zablocka, M., Röttgers, R., Thomas, R., 2013. Composition of dissolved organic matter along an Atlantic Meridional Transect from fluorescence spectroscopy and parallel factor analysis. Mar. Chem. 157, 170–184. https://doi.org/10.1016/j.marchem.2013.10.004.

Kuypers, M.M.M., Marchant, H.K., Kartal, B., 2018. The microbial nitrogen-cycling network. Nat. Rev. Microbiol. 16, 263–276. https://doi.org/10.1038/nrmicro.2018.9.

Lawaetz, A.J., Stedmon, C.A., 2009. Fluorescence intensity calibration using the Raman scatter peak of water. Appl. Spectrosc. 63, 936–940.

Lusk, M.G., Toor, G.S., 2016a. Biodegradability and molecular composition of dissolved organic nitrogen in urban stormwater runoff and outflow water from a stormwater retention pond. Environ. Sci. Technol. 50, 3391–3398. https://doi.org/10.1021/acs.est.5b05714.

Lusk, M.G., Toor, G.S., 2016b. Dissolved organic nitrogen in urban streams: biodegradability and molecular composition studies. Water Res. 96, 225–235. https://doi.org/10.1016/j.watres.2016.03.060.

Murphy, K.R., Hambly, A., Singh, S., Henderson, R.K., Baker, A., Stuetz, R., et al., 2011. Organic matter fluorescence in municipal water recycling schemes: toward a unified PARAFAC model. Environ. Sci. Technol. 45, 2909–2916. https://doi.org/10.1021/es103015e.

Murphy, K.R., Stedmon, C.A., Graeber, D., Bro, R., 2013. Fluorescence spectroscopy and multi-way techniques. PARAFAC. Anal. Methods 5, 6557–6566. https://doi.org/10.1039/c3ay41160e.

Murphy, K.R., Stedmon, C.A., Wenig, P., Bro, R., 2014. OpenFluor–an online spectral library of auto-fluorescence by organic compounds in the environment. Anal. Methods 6, 658–661. https://doi.org/10.1039/c3ay41935e.

Murphy, K.R., Timko, S.A., Gonsior, M., Powers, L.C., Wunsch, U.J., Stedmon, C.A., 2018. Photochemistry illuminates ubiquitous organic matter fluorescence spectra. Environ. Sci. Technol. 52, 11243–11250. https://doi.org/10.1021/acs.est.8b02648.

Ohno, T., Parr, T.B., Gruselle, M.C., Fernandez, I.J., Sleighter, R.L., Hatcher, P.G., 2014. Molecular composition and biodegradability of soil organic matter: a case study comparing two new England forest types. Environ. Sci. Technol. 48, 7229–7236. https://doi.org/10.1021/es405570c.

Osburn, C.L., Wigdahl, C.R., Fritz, S.C., Saros, J.E., 2011. Dissolved organic matter composition and photoreactivity in prairie lakes of the U.S. Great Plains. Limnol. Oceanogr. 56, 2371–2390. https://doi.org/10.4319/lo.2011.56.6.2371.

Osburn, C.L., Handsel, L.T., Peierls, B.L., Paerl, H., 2016. Predicting sources of dissolved organic nitrogen to an estuary from an agro-urban coastal watershed. Environ. Sci. Technol. 50, 8473–8484. https://doi.org/10.1021/acs.est.6b00053.

Qin, B., Xu, P., Wu, Q., Luo, L., Zhang, Y., 2007. Environmental issues of Lake Taihu, China. Hydrobiologia 581, 3–14. https://doi.org/10.1007/s10750-006-0521-5.

Rosamond, M.S., Thuss, S.J., Schiff, S.L., 2012. Dependence of riverine nitrous oxide emissions on dissolved oxygen levels. Nat. Geosci. 5, 715–718.

Shen, Y., Fichot, C.G., Benner, R., 2012. Floodplain influence on dissolved organic matter composition and export from the Mississippi-Atchafalaya River system to the Gulf of Mexico. Limnol. Oceanogr. 57, 1149–1160. https://doi.org/10.4319/lo.2012.57.4.1149.

Song, K., Shang, Y., Wen, Z., Jacinthe, P.-A., Liu, G., Lyu, L., et al., 2018. Characterization of CDOM in saline and freshwater lakes across China using spectroscopic analysis. Water Res. 150, 403–417. https://doi.org/10.1016/j.watres.2018.12.004.

Soued, C., del Giorgio, P.A., Maranger, R., 2015. Nitrous oxide sinks and emissions in boreal aquatic networks in Québec. Nat. Geosci. 9, 116–120. https://doi.org/10.1038/ngeo2611.

Spencer, R.G.M., Butler, K.D., Aiken, G.R., 2012. Dissolved organic carbon and chromophoric dissolved organic matter properties of rivers in the USA. J. Geophys. Res. 117, G03001. https://doi.org/10.1029/2011jg001928.

Spencer, R.G.M., Aiken, G.R., Dornblaser, M.M., Butler, K.D., Holmes, R.M., Fiske, G., et al., 2013. Chromophoric dissolved organic matter export from U.S. rivers. Geophys. Res. Lett. 40, 1575–1579. https://doi.org/10.1002/grl.50357.

Spencer, R.G.M., Guo, W., Raymond, P.A., Dittmar, T., Hood, E., Fellman, J., et al., 2014. Source and biolability of ancient dissolved organic matter in glacier and lake ecosystems on the Tibetan Plateau. Geochim. Cosmochim. Acta 142, 64–74. https://doi.org/10.1016/j.gca.2014.08.006.

Stedmon, C.A., Bro, R., 2008. Characterizing dissolved organic matter fluorescence with parallel factor analysis: a tutorial. Limnol. Oceanogr. Methods 6, 572–579. https://doi.org/10.4319/lom.2008.6.572b.

Stedmon, C.A., Markager, S., 2005. Resolving the variability in dissolved organic matter fluorescence in a temperate estuary and its catchment using PARAFAC analysis. Limnol. Oceanogr. 50, 686–697. https://doi.org/10.4319/lo.2005.50.2.0686.

Stedmon, C.A., Markager, S., Bro, R., 2003. Tracing dissolved organic matter in aquatic environments using a new approach to fluorescence spectroscopy. Mar. Chem. 82, 239–254. https://doi.org/10.1016/s0304-4203(03)00072-0.

Stedmon, C.A., Thomas, D.N., Granskog, M., Kaartokallio, H., Papadimitriou, S., Kuosa, H., 2007. Characteristics of dissolved organic matter in Baltic coastal sea ice: allochthonous or autochthonous origins? Environ. Sci. Technol. 41, 7273–7279. https://doi.org/10.1021/es071210f.

Stedmon, C.A., Thomas, D.N., Papadimitriou, S., Granskog, M.A., Dieckmann, G.S., 2011. Using fluorescence to characterize dissolved organic matter in Antarctic sea ice brines. J. Geophys. Res. 116, G03027. https://doi.org/10.1029/2011jg001716.

Stubbins, A., Spencer, R.G.M., Chen, H., Hatcher, P.G., Mopper, K., Hernes, P.J., et al., 2010. Illuminated darkness: molecular signatures of Congo River dissolved organic matter and its photochemical alteration as revealed by ultrahigh precision mass spectrometry. Limnol. Oceanogr. 55, 1467–1477. https://doi.org/10.4319/lo.2010.55.4.1467.

Stubbins, A., Hood, E., Raymond, P.A., Aiken, G.R., Sleighter, R.L., Hernes, P.J., et al., 2012. Anthropogenic aerosols as a source of ancient dissolved organic matter in glaciers. Nat. Geosci. 5, 198–201. https://doi.org/10.1038/ngeo1403.

Tang, X., Gao, G., Chao, J., Wang, X., Zhu, G., Qin, B., 2010. Dynamics of organic-aggregate-bacterial communities and related environmental factors in Lake Taihu, a large eutrophic shallow lake in China. Limnol. Oceanogr. 55, 469–480.

Tang, X., Chao, J., Gong, Y., Wang, Y., Wilhelm, S.W., Gao, G., 2017. Spatiotemporal dynamics of bacterial community composition in large shallow eutrophic Lake Taihu: high overlap between free-living and particle-attached assemblages. Limnol. Oceanogr. 62, 1366–1382. https://doi.org/10.1002/lno.10502.

Turner, P.A., Griffis, T.J., Lee, X., Baker, J.M., Venterea, R.T., Wood, J.D., 2015. Indirect nitrous oxide emissions from streams within the US Corn Belt scale with stream order. Proc. Natl. Acad. Sci. 112, 9839–9843.

Vizzini, S., Savona, B., Chi, T.D., Mazzola, A., 2005. Spatial variability of stable carbon and nitrogen isotope ratios in a Mediterranean coastal lagoon. Hydrobiologia 550, 73–82. https://doi.org/10.1007/s10750-005-4364-2.

Vonk, J.E., Tank, S.E., Mann, P.J., Spencer, R.G.M., Treat, C.C., Striegl, R.G., et al., 2015. Biodegradability of dissolved organic carbon in permafrost soils and aquatic systems: a meta-analysis. Biogeosciences 12, 6915–6930. https://doi.org/10.5194/bg-12-6915-2015.

Walker, S.A., Amon, R.M.W., Stedmon, C., Duan, S., Louchouarn, P., 2009. The use of PARAFAC modeling to trace terrestrial dissolved organic matter and fingerprint water masses in coastal Canadian Arctic surface waters. Journal of Geophysical Research-Biogeosciences 114, G00F06. https://doi.org/10.1029/2009jg000990.

Weishaar, J.L., Aiken, G.R., Bergamaschi, B.A., Fram, M.S., Fujii, R., Mopper, K., 2003. Evaluation of specific ultraviolet absorbance as an indicator of the chemical composition of reactivity of dissolved organic matter. Environ. Sci. Technol. 37, 4702–4708.

Wen, Z., Song, K., Shang, Y., Fang, C., Li, L., Lv, L., et al., 2017. Carbon dioxide emissions from lakes and reservoirs of China: a regional estimate based on the calculated pCO2. Atmos. Environ. 170, 71–81.

Weyhenmeyer, G.A., Kosten, S., Wallin, M.B., Tranvik, L.J., Jeppesen, E., Roland, F., 2015. Significant fraction of CO2 emissions from boreal lakes derived from hydrologic inorganic carbon inputs. Nat. Geosci. 8, 933–936. https://doi.org/10.1038/ngeo2582.

Wik, M., Varner, R.K., Anthony, K.W., MacIntyre, S., Bastviken, D., 2016. Climate-sensitive northern lakes and ponds are critical components of methane release. Nat. Geosci. 9, 99–105. https://doi.org/10.1038/ngeo2578.

Williams, C.J., Yamashita, Y., Wilson, H.F., Jaffé, R., Xenopoulos, M.A., 2010. Unraveling the role of land use and microbial activity in shaping dissolved organic matter characteristics in stream ecosystems. Limnol. Oceanogr. 55, 1159–1171. https://doi.org/10.4319/lo.2010.55.3.1159.

Williams, C.J., Frost, P.C., Morales-Williams, A.M., Larson, J.H., Richardson, W.B., Chiandet, A.S., et al., 2016. Human activities cause distinct dissolved organic matter composition across freshwater ecosystems. Glob. Chang. Biol. 22, 613–626. https://doi.org/10.1111/gcb.13094.

Wu, H., Li, X., Li, J., Jiang, Z., Li, G., Liu, L., 2015. Evaporative enrichment of stable isotopes (δ18O and δD) in lake water and the relation to lake-level change of Lake Qinghai, Northeast Tibetan Plateau of China. Journal of Arid Land 7, 623–635. https://doi.org/10.1007/s40333-015-0048-6.

Wünsch, U.J., Murphy, K.R., Stedmon, C.A., 2017. The one-sample PARAFAC approach reveals molecular size distributions of fluorescent components in dissolved organic matter. Environ. Sci. Technol. 51, 11900–11908. https://doi.org/10.1021/acs.est.7b03260.

Xiao, W., Wen, X., Wang, W., Xiao, Q., Xu, J., Cao, C., et al., 2016. Spatial distribution and temporal variability of stable water isotopes in a large and shallow lake. Isot. Environ. Health Stud. 52, 443–454. https://doi.org/10.1080/10256016.2016.1147442.

Xiao, Q., Xu, X., Zhang, M., Duan, H., Hu, Z., Wang, W., et al., 2018. Coregulation of nitrous oxide emissions by nitrogen and temperature in China's third largest freshwater lake (Lake Taihu). Limnol. Oceanogr. 64, 1070–1086. https://doi.org/10.1002/lno.11098.

Xu, H., Cai, H., Yu, G., Jiang, H., 2013. Insights into extracellular polymeric substances of cyanobacterium Microcystis aeruginosa using fractionation procedure and parallel factor analysis. Water Res. 47, 2005–2014.

Yang, L., Hur, J., 2014. Critical evaluation of spectroscopic indices for organic matter source tracing via end member mixing analysis based on two contrasting sources. Water Res. 59, 80–89. https://doi.org/10.1016/j.watres.2014.04.018.

Yang, L., Hong, H., Guo, W., Arthur Chen, C.-T., Pan, P.-I., Feng, C.-C., 2012. Absorption and fluorescence of dissolved organic matter in submarine hydrothermal vents off NE Taiwan. Mar. Chem. 128–129, 64–71. https://doi.org/10.1016/j.marchem.2011.10.003.

Yang, L., Zhuang, W.E., Chen, C.A., Wang, B.J., Kuo, F.W., 2017. Unveiling the transformation and bioavailability of dissolved organic matter in contrasting hydrothermal vents using fluorescence EEM-PARAFAC. Water Res. 111, 195–203. https://doi.org/10.1016/j.watres.2017.01.001.

Yu, Z., Deng, H., Wang, D., Ye, M., Tan, Y., Li, Y., et al., 2013. Nitrous oxide emissions in the Shanghai river network: implications for the effects of urban sewage and IPCC methodology. Glob. Chang. Biol. 19, 2999–3010.

Zarnetske, J.P., Haggerty, R., Wondzell, S.M., Bokil, V.A., González-Pinzón, R., 2012. Coupled transport and reaction kinetics control the nitrate source-sink function of hyporheic zones. Water Resour. Res. 48, W11508. https://doi.org/10.1029/2012WR011894.

Zhang, Y., van Dijk, M.A., Liu, M., Zhu, G., Qin, B., 2009. The contribution of phytoplankton degradation to chromophoric dissolved organic matter (CDOM) in eutrophic shallow

lakes: field and experimental evidence. Water Res. 43, 4685–4697. https://doi.org/ 10.1016/j.watres.2009.07.024.

Zhou, Y., Shi, K., Zhang, Y., Jeppesen, E., Liu, X., Zhou, Q., et al., 2017. Fluorescence peak integration ratio IC:IT as a new potential indicator tracing the compositional changes in chromophoric dissolved organic matter. Sci. Total Environ. 574, 1588–1598. https:// doi.org/10.1016/j.scitotenv.2016.08.196.

Zhou, Y., Davidson, T.A., Yao, X., Zhang, Y., Jeppesen, E., de Souza, J.G., et al., 2018a. How autochthonous dissolved organic matter responds to eutrophication and climate warming: evidence from a cross-continental data analysis and experiments. Earth Sci. Rev. 185, 928–937. https://doi.org/10.1016/j.earscirev.2018.08.013.

Zhou, Y., Xiao, Q., Yao, X., Zhang, Y., Zhang, M., Shi, K., et al., 2018b. Accumulation of terrestrial dissolved organic matter potentially enhances dissolved methane levels in eutrophic Lake Taihu, China. Environ. Sci. Technol. 52, 10297–10306. https://doi. org/10.1021/acs.est.8b02163.

Zhou, Y., Yao, X., Zhang, Y., Zhang, Y., Shi, K., Tang, X., et al., 2018c. Response of dissolved organic matter optical properties to net inflow runoff in a large fluvial plain lake and the connecting channels. Sci. Total Environ. 639, 876–887. https://doi.org/10.1016/j. scitotenv.2018.05.180.